J. Physiol. (1984), **348**, *pp.* 341–367
With 14 text-figures
Printed in Great Britain

CHARACTERIZATION OF THE PACE-MAKER CURRENT KINETICS IN CALF PURKINJE FIBRES

BY DARIO DIFRANCESCO

From the Dipartimento di Fisiologia e Biochimica Generali, Elettrofisiologia, via Celoria 26, 20133 Milano, Italy

(*Received 9 May 1983*)

SUMMARY

1. Kinetics of the cardiac pace-maker current (i_f) were studied using high K^+, low Na^+ solutions under conditions where the current time course could be dissected from other components.

2. Activation of i_f during relatively large negative pulses is S-shaped, and is approximated by an exponential function of time to the third power. Less-pronounced S-shaped activation occurs at potentials close to the middle of the activation curve (near $-70/-80$ mV). Here, allowing for the presence of a very slow component, the power required to fit the current activation approaches 1.

3. The comparison between current activation and deactivation at the same potentials shows that although deactivation can be approximated by a single exponential, the two processes have a quite different time dependence, and this difference depends on the membrane potential. This behaviour is not compatible with Hodgkin–Huxley kinetics.

4. While near the half-activation range the current decays with an apparently single exponential time course, at more positive potentials the current deactivation becomes sigmoidal. At least the third power of an exponential is required to fit its time course at potentials positive to about -40 mV. These data imply that both open and closed states correspond to several distinct channel configurations.

5. The 'delay' in the current onset during a hyperpolarization is decreased by applying large, short hyperpolarizations before activation. Suitable pre-pulse durations and/or amplitudes can reduce the subsequent current activation to a single exponential. Records with and without a pre-pulse do not always superimpose.

6. After the activation 'delay' has been removed by a suitable hyperpolarization preceding an activating pulse, the time course of its recovery can be studied by applying depolarizations of given amplitude and variable duration. The time course of the delay recovery does not seem to be linked to the time course of current deactivation recorded at the same voltage.

7. Reduction of the activation 'delay' by conditioning pre-hyperpolarizations does not affect current decay during a subsequent depolarizing pulse. The current decay appears to depend only on the current amplitude reached before a deactivating pulse is applied. This, and the evidence in the preceding paragraph, suggest that the delay recovery and the current deactivation are independent processes.

8. A reaction scheme is proposed, which has been developed on the basis of the experimentally determined kinetic properties of i_f. The channel model is composed of five gating subunits of three different types, not all independent in their movements.

9. The properties of the gating subunits and their dependence on voltage have been defined by experimental data fitting. The model satisfactorily predicts the current time course on activation and deactivation, and its kinetic behaviour during different voltage-clamp protocols. The aim and limits of the proposed model, which is to be considered as only a descriptive one, are discussed.

INTRODUCTION

In the heart, as in other excitable tissues, the kinetics of most membrane currents can be described in terms of Hodgkin–Huxley channel models (Trautwein, 1973; McAllister, Noble & Tsien, 1975; Beeler & Reuter, 1977; D. DiFrancesco & D. Noble, 1984, unpublished observations). These models, as originally formulated by Hodgkin & Huxley (1952), are based on the assumption that channel opening/closing processes are attributable to otherwise unidentified gating subunits that move within the membrane under the effect of the electric field. The gating subunits are identical and independent of each other. Although the basic idea of charged groups translating (or rotating) to gate the channel opening/closing processes when the electric field is changed has been successfully applied to a variety of excitable membranes, there is evidence that Hodgkin–Huxley models in their simplest form fail to account for some of the kinetic properties of K^+ and Na^+ currents in different tissues (Goldman & Schauf, 1973; Palti, Ganot & Stämpfli, 1976; Bezanilla & Armstrong, 1977; Begenisich, 1979).

A description of the kinetics of the Purkinje fibre pace-maker current was first given by Noble & Tsien (1968) in terms of a single Hodgkin–Huxley gating parameter. An obvious consequence of the reinterpretation of the ionic nature of this current (DiFrancesco, 1981*a*) is the need for a detailed study of its kinetic properties under unperturbed conditions. This is also suggested by the observation that first, the presence of fast depletion of cleft K^+ ions during negative voltage pulses can overlap i_f activation and distort its time course, particularly at short times after a pulse onset, and secondly, that the use of Ba^{2+} to reduce interference of K^+ accumulation/depletion phenomena allows i_f kinetics to be investigated over a much broader voltage range than was previously possible.

This paper is the continuation of a series of papers devoted to the study of the newly interpreted cardiac pace-maker current, i_f (DiFrancesco, 1981*a*, *b*, 1982), and aims to characterize in some detail the kinetic properties of i_f. It is divided into two parts. In the first part, experimental results are presented showing how both activation and deactivation of i_f are S-shaped functions of time, and how the i_f kinetic behaviour is influenced by the voltage protocol used to study it. These data indicate that Hodgkin–Huxley models are insufficient to describe i_f kinetics. Following the indications inferred from the results of the first part, in the second part a channel model is developed and its predictions are compared with the experimental data.

METHODS

The methods and apparatus for voltage clamping short, unbranched Purkinje fibres from calf hearts have been described previously (DiFrancesco, 1981*a*, *b*, 1982). The standard Tyrode solution used contained (in mM): NaCl, 35; KCl, 20; Tris HCl (or choline Cl), 105; $CaCl_2$, 1·8; $MgCl_2$, 2; it was buffered by Tris HCl to pH 7·4, and continuously bubbled with O_2. $BaCl_2$ and $MnCl_2$ were routinely added in concentrations of 5 mM each to block i_{K1} and i_{si} respectively. The above K^+ and Na^+ concentrations have been used in all the experiments where a complete set of data was collected for comparison with theoretical predictions (see Part II of Results). Although in this paper a systematic study of the effect of ion concentrations on i_f kinetics was not carried out, the i_f behaviour has been observed in the range 3–50 mM-K^+ and 14–70 mM-Na^+. In this range the i_f kinetic properties are qualitatively similar to those reported at the standard K^+ and Na^+ concentrations. Voltage and current traces were recorded during experiments on an FM recorder (HP 3964A). Corner low-pass frequency was 1250 or 2500 Hz. Current traces were subsequently digitized in records of up to 2 K data points using a 12-bit A/D converter built in our laboratory. The sampling frequency could be varied between 30 and 8600 Hz and was selected according to the speed of current change to be converted. Three current records corresponding to the same voltage pulse were normally averaged before storage on disk. Digital manipulation and plotting were then performed using a desk computer system (HP-85 and HP-7225). Electronic analog subtraction of linear background and capacity currents was sometimes used. The method consisted of subtracting from the total recorded current during a small voltage-clamp pulse (±10 mV) a component obtained by suitable amplification and derivation (three RC circuits) of the applied voltage signal, until a flat record resulted. During larger negative pulses which elicited i_f activation, the linear time-independent and capacity components were thus automatically subtracted. Given the relatively slow kinetics of i_f with respect to capacity transients, this procedure was not always necessary and was not used routinely.

Data fitting

Data fitting using the reaction scheme shown in Part II of Results (Fig. 10) was achieved by step integration of the matrix differential equation

$$dp/dt = Ap + k, \tag{1}$$

p being the probability vector of the channel configuration ensemble reduced by one dimension,

$$p = [p_1 p_2 p_3 \ldots p_7] \tag{2}$$

and A being the matrix

$$A = \begin{bmatrix} -\alpha_x-2\alpha_y & \beta_x & \beta_y & 0 & 0 & 0 & 0 \\ \alpha_x & -\beta_x-2\alpha_y & 0 & \beta_y & 0 & 0 & 0 \\ 2\alpha_y & 0 & -\alpha_x-\alpha_y-\beta_y & \beta_x & 2\beta_y & 0 & 0 \\ 0 & 2\alpha_y & \alpha_x & -\alpha_y-\beta_x-\beta_y & 0 & 2\beta_y & 0 \\ 0 & 0 & \alpha_y & 0 & -\alpha_x-2\beta_y & \beta_x & 0 \\ 0 & 0 & 0 & \alpha_y & \alpha_x & -2\alpha_z-\beta_x-2\beta_y & \beta_z \\ -2\beta_z & -2\beta_z & -2\beta_z & -2\beta_z & -2\beta_z & 2\alpha_z-2\beta_z & -\alpha_z-3\beta_z \end{bmatrix}. \tag{3}$$

The meaning of the rate constants α_j, β_j, where $j = x, y, z$ is given in Fig. 10. Time constants (τ) and activation fractions as reported in Fig. 14 are related to the rate constants by the usual equations:

$$\tau_j = 1/(\alpha_j+\beta_j) \tag{4a}$$

$$j = \beta_j/(\alpha_j+\beta_j) \quad (j = x, y, z). \tag{4b}$$

Steady-state conditions were obtained by the equation

$$p_\infty = A^{-1}k, \tag{5}$$

k being the vector

$$k = [0\ 0\ 0\ 0\ 0\ 0\ 2\beta_z]. \tag{6}$$

The general treatment of kinetic systems from which the above equations derive is given in the Appendix. Initial conditions, that is the initial state probability vector p_0 in a clamp pulse, were calculated using the relation (5) with values of rate constants in A^{-1} and k taken at the reference potential. Each time-dependent current change corresponding to a voltage-clamp pulse from say E_1 to E_2 is completely characterized in the model by giving values of *all* the rate constants at E_1 and E_2, and the experimentally measurable value of i_f at both voltages. The twelve free parameters thus needed are far too many, but can often be reduced if one of the voltages is at either extreme of the i_f activation range, as explained in more detail in Part II of Results. Further restrictions come from the use of protocols more complex than single-pulse experiments, where one set of parameters – corresponding to a given voltage – is used to fit several types of measurements involving the same voltage. Examples of this are the two-pulse experiments shown in Figs. 11*B*, 12 and 13*B*, *C*, and the three-pulse experiments shown in Figs. 11*C*, *D* and 13*D*. Fitting of experiments of this kind necessarily started from the measurement of the i_f activation curve $f_\infty(E)$ (the use of the symbol f to express the current activation variable is justified later: see Results). This was done with the usual two-pulse method, consisting of applying hyperpolarizations from a holding potential of around −40 mV to various voltage levels for times long enough for steady state to be reached (an illustration of the different durations at different potentials is given in Fig. 13) and subsequently applying a test pulse either to a large negative potential to record the residual current activation, or to a depolarized potential to record the current decay. The amplitude of test records was then measured automatically by the computer on the mean trace from three identical pulses. Examples of $f_\infty(E)$ curves are given in Fig. 14.

Curve fitting during activation on large hyperpolarizations or during deactivation on large depolarizations applied after full activation was performed first, because it required well-defined initial and final conditions ($x, y, z = 1$ at approximately $E < -130$ mV, and $x, y, z = 0$ at approximately $E > -30$ mV: see Fig. 14), and thus a reduction of free variables as mentioned above. Fitting of activation/deactivation records in the intermediate voltage range and of two- or three-pulse protocol records was then performed by progressive extrapolation of the values previously selected. The parameters giving the best possible fitting and values of f_∞ as close as possible to those determined experimentally were selected. All the parameters used in curve fitting for three experiments have been plotted in Fig. 14. The integration step Δt in the differential eqn. (1) was a critical factor in the computation, and steps that were too large led to instability. This was strongly dependent on the values of time constants. Even when no instability was evident, moderate deviations from a stable response could be elicited by increasing Δt. This problem was solved by running a reference computation with a very short Δt, and then selecting the largest possible value of Δt that gave an identical response. Values of Δt were usually 5×10^{-4} to 10^{-2} times the total integration time. Larger plotting steps were used in the fitting curves shown in the Results (Figs. 11–13).

The need for reproducing sets of data spanning a relatively large voltage range and obtained with different protocols made it more difficult to choose a suitably fast and valid best-fitting algorithm. Thus, all data fitting is not to be considered as a proper best-fitting procedure and was done by eye. It should be added, however, that even slight changes in the selected parameters usually caused large deviations from the experimental records, and that attempts to reproduce experimental data made over some 500 curves from fourteen experiments have proved convincingly that the relative positions and amplitudes of the activation curves and of the time constant curves as given in Fig. 14 are carefully selected. This obviously does not exclude the possibility that models other than, and possibly more complex than, the one explored here (Fig. 10) could give more satisfactory data reproduction.

RESULTS

Part I. Experimental study of the properties of i_f kinetics

Sigmoid nature of i_f activation

The time course of activation of i_f during hyperpolarization in the range −95 to −135 mV is shown in Fig. 1 using linear (upper panels) or semilogarithmic plots (lower panels). In both representations the sigmoid nature of the current onset is apparent. The current behaves as a single exponential only after an initial 'delay',

the value of which is strongly voltage dependent and decreases at more negative potentials. This time course is also compatible, on the other hand, with an exponential to a power $n > 1$. However, as shown later (Figs. 3 and 4), there is no single value of n able to fit the current activation at all potentials. In the records of Fig. 1 the linear leak and capacitive components have been subtracted electronically (see

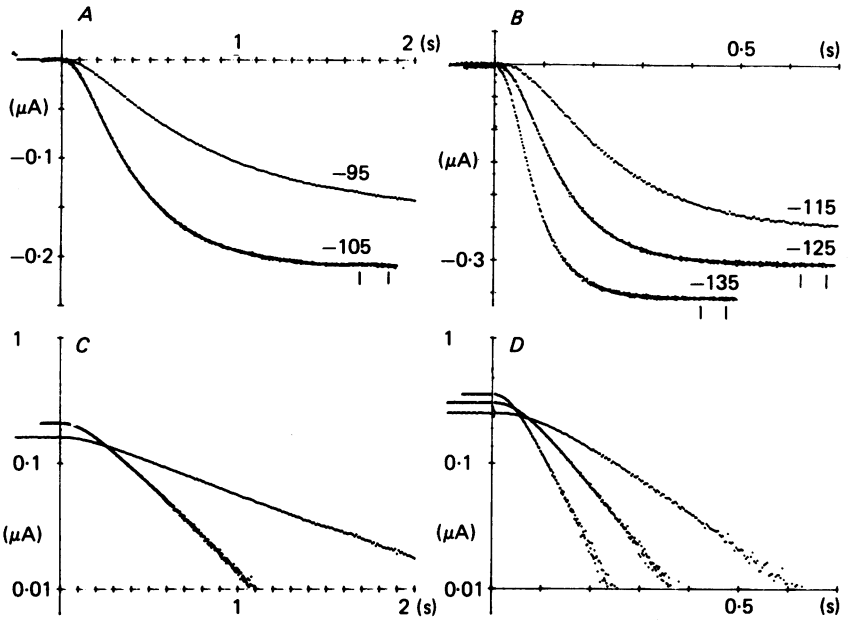

Fig. 1. Activation of i_f at −95 and −105 mV (*A*) and at −115, −125 and −135 mV (*B*) from a holding potential of −45 mV. Linear leak and capacitive components have been subtracted. *C* and *D*, the difference $i_f - i_{f\infty}$ is plotted on a semilogarithmic scale. Steady-state levels obtained by averaging the corresponding current within bars in *A* and *B*. Bars out of scale for the −95 and −115 mV records.

Methods), and the fact that all records start at the absolute zero current level thus indicates good linearity of the background component down to −135 mV in this preparation. Further direct evidence of a sigmoidal i_f activation comes from envelope test experiments as shown in Fig. 2. Similar results have already appeared (see Fig. 1 in DiFrancesco, 1982), but here a better resolution has been obtained by averaging three pulses for each trace, and by using a finer grid of pulse durations. Activation at −114 (*A*) and −104 mV (*B*) is shown together with the tails recorded on depolarizing to −19 mV after pulses of variable duration in the range 2–1500 ms. The S-shaped current onset is more evident from the tail envelopes in the enlarged plots of the lower panels. These plots confirm that the sigmoid nature of the current onset is a genuine property of i_f, and that i_f activation occurs according to kinetics more complex than first-order.

Dissection of i_f during activation on large negative pulses using Cs^+

The blocking action of Cs^+ on i_f at very negative potentials (DiFrancesco, 1982) can be used to isolate the current i_f from other components during activation upon

hyperpolarization. Two conditions are required for a satisfactory current dissection: first, the block of i_f by Cs^+ should be highly specific (that is, i_f must be the only current blocked by Cs^+); and secondly, the block itself must be complete. The latter condition can be easily fulfilled by using relatively high concentrations of the blocking ion, and by restricting the analysis to a negative-enough voltage range. As for the

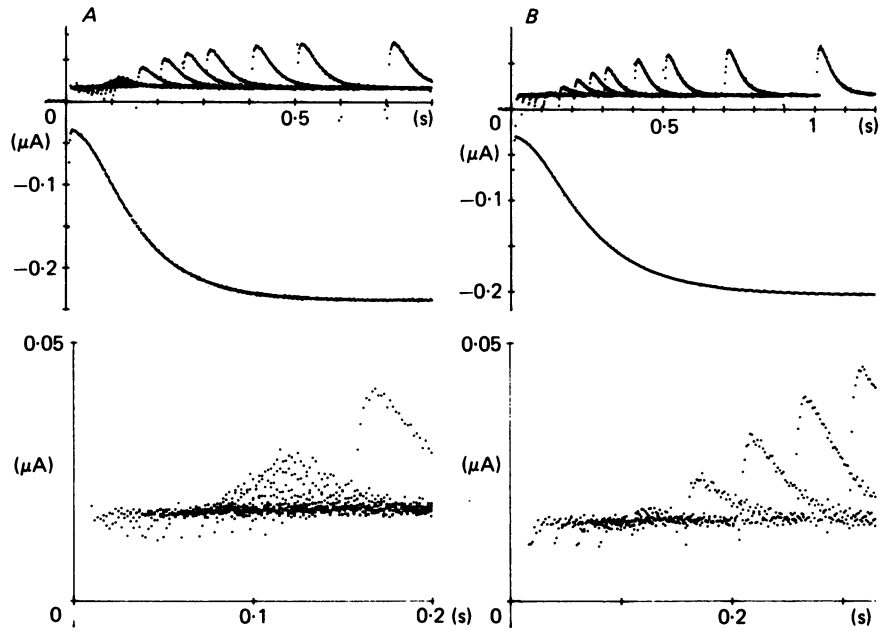

Fig. 2. Envelope tests during current activation. From the holding potential of −34 mV pulses to −114 (*A*) and −104 mV (*B*) of various durations in the range 2–1500 ms are followed by a 300 ms depolarization to −19 mV. In the upper panels the current activation during 1500 ms pulses and the tails at −19 mV are shown. A better resolution of the S-shaped tails envelope is obtained by enlarging current and time scales in the lower panels. The tail amplitude is not appreciably different from zero after hyperpolarizing pulses of duration up to about 70 ms at −114 mV (*A*), and up to about 100 ms at −104 mV (*B*).

former condition, it is known that in Purkinje fibres Cs^+ blocks the K^+ background i_{K1} current as well as i_f. However, while concentrations of less than 20 mM are said to have little action on i_{K1} (Isenberg, 1976), 1 mM-Cs^+ is enough to give a substantial i_f reduction at potentials around −100 mV. Also, the fraction of i_{K1} unblocked in Ba^{2+}-containing solutions is negligible (DiFrancesco, 1981*a*, 1982), as indirectly confirmed by the linearity of the residual background component after Ba^{2+} in the negative voltage region (see for example Figs. 1 and 9). Therefore it can be safely assumed that in the presence of Ba^{2+} and using a suitable Cs^+ concentration (5 mM in Fig. 3), the block of i_f by Cs^+ during pulses negative to about −100 mV is fairly specific. Fig. 3 shows a set of current records during hyperpolarizations to the range −90 to −130 mV from a holding potential of −40 mV in a control solution (records marked by upper-case letters in *A*) and after addition of 5 mM-CsCl (lower-case letters). Subtraction of traces in the presence of Cs^+ from those in the control solution

yields the Cs^+-dependent current traces given in panel *B*. The Cs^+-dependent current is nil at the holding potential and at the start of each pulse, indicating that i_f is fully deactivated at −40 mV, and that the Cs^+-induced blockade is highly specific under these circumstances.

An indication of the extent by which i_f activation deviates from simple exponential behaviour is given by plotting in the lower panels of Fig. 3 the variable

$$r(t) = 1-(i(t)/i_\infty)^{1/n},$$

i_∞ being the steady-state current value, on a semilogarithmic scale. In the traditional Hodgkin–Huxley (1952) description an exponential dependence of r on

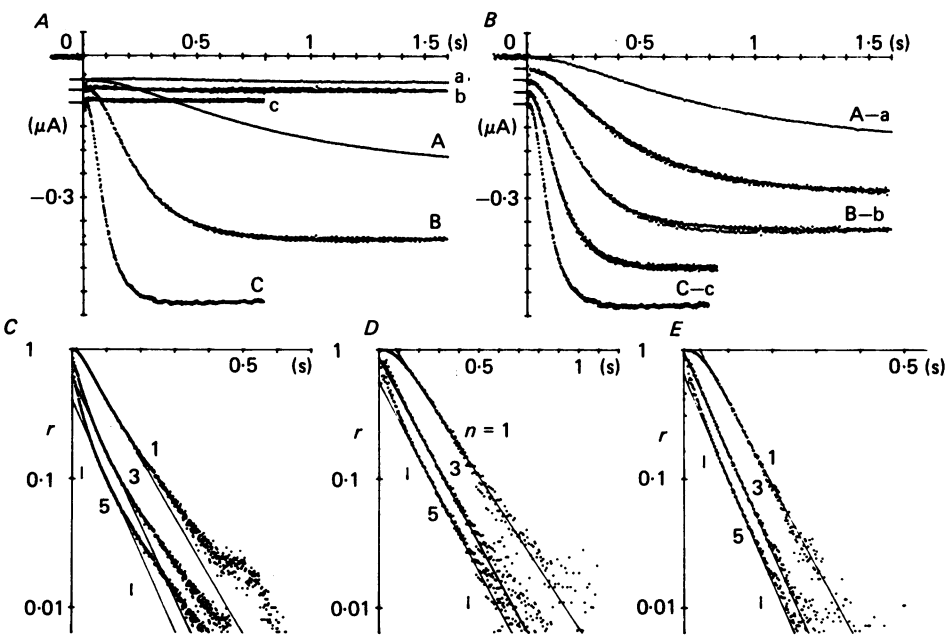

Fig. 3. *A*, current recorded on activation to −90, −110 and −130 mV from a holding potential of −40 mV before (A, B, C) and during (a, b, c) perfusion with 5 mM-CsCl. *B*, records obtained by subtraction of the Cs^+ traces from corresponding control traces during pulses to −90, −100, −110, −120 and −130 mV. The traces are shifted downwards in 25 nA steps for clarity (zero current level marked in each case by a horizontal trace). *C* to *E*, plots of $\ln r(t) = \ln(1-(i(t)/i_\infty)^{1/n})$ for the −90 (*C*), −110 (*D*) and −130 mV (*E*) pulse records. The plots corresponding to $n = 1$, 3 and 5 have been reported for each trace, as indicated. Best-fitting lines through points within bars give the following intercepts at $t = 0$ for $n = 1$, 3 and 5 respectively: *C*, 0·40, 0·61 and 1·15; *D*, 0·55, 0·86 and 1·60; *E*, 0·63, 0·95 and 1·70. In this experiment the external K^+ concentration was 30 mM.

time is obtained when n is given an appropriate integer value, corresponding to the number of independent subunits taking part in the gating process. The $r(t)$ plots in Fig. 3 correspond to pulses to −90 (*C*), −110 (*D*) and −130 mV (*E*), and at each potential have been reported for the n values of 1, 3 and 5 (intermediate values of 2 and 4, also checked, are omitted for clarity). At −110 and −130 mV (*D* and *E*), the plots with $n = 3$ are approximately linear and cross the ordinate near the value $r = 1$, suggesting that a Hodgkin–Huxley model with $n = 3$ could be appropriate for

describing i_f kinetics at these potentials. At more depolarized voltages, however, large deviations from a straight line are observed in the semilogarithmic plot with $n = 3$ (panel C), and the current time course is better approximated by $n = 1$, indicating single-exponential behaviour. These data exclude the possibility that a Hodgkin–Huxley model, with a given value of n, can account for i_f kinetics during activation. Results similar to those shown in Fig. 3 can be obtained by dissecting the i_f time course from other components using the electronic subtraction procedure mentioned in Methods (see Fig. 1) rather than the Cs^+-block procedure. In none of the twelve experiments where activation was measured could the current time course be properly fitted by a single value of n.

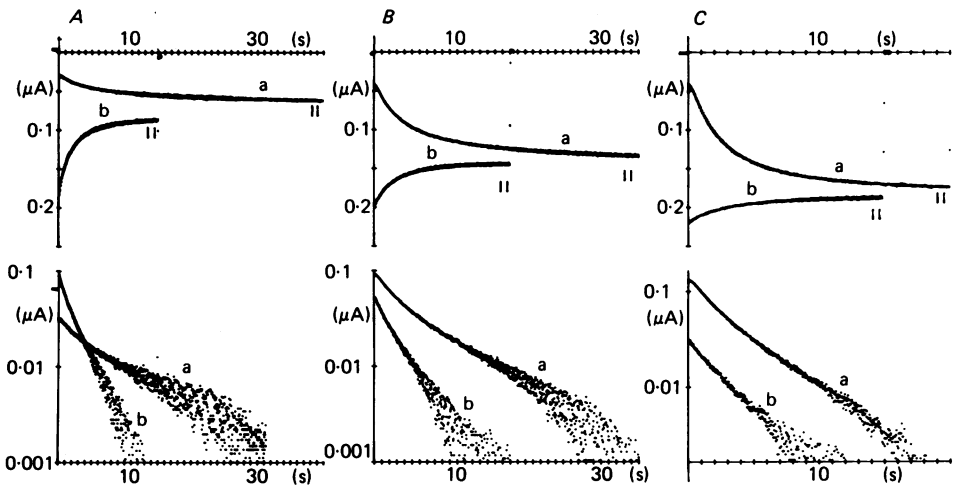

Fig. 4. Activation and deactivation time course of i_f at -70 (A), -75 (B) and -80 mV (C). Pulses are either from the holding potential of -40 mV (a) or after an 800 ms pulse to -130 mV (b). The lower panels show semilogarithmic plots of $i_f - i_{f\infty}$.

i_f kinetics near the current half-activation range

Further information on i_f kinetics is obtained by comparing the current time course during activation and deactivation at the same potential. In the case of simple, first-order kinetics an identical single-exponential time dependence is expected during depolarization and hyperpolarization to a given potential. On the other hand, Hodgkin–Huxley models with two or more gating subunits and where the open state corresponds to one channel configuration only give rise – as is easily shown – to an activation time course slower than the corresponding deactivation time course. Current traces recorded during pulses to near the half-activation voltage range either from the holding potential of -40 mV or after current activation at -130 mV are shown in Fig. 4 (upper panels). From the semilogarithmic plots in the lower panels of Fig. 4 two features of the current kinetics are apparent: first, a slow component seems to be present, particularly in the activation time dependence, which develops according to the sum of at least two exponentials; and secondly, while near the top of the activation curve (panel C) activation and deactivation time courses do not greatly differ (although a slow component and an initial short delay are visible in current activation), at less negative potentials (panels A and B) current activation

becomes clearly slower than deactivation. Similar data have been observed in six more experiments. These data are inconsistent with single or multi-variable Hodgkin–Huxley kinetics.

Time course of i_f during deactivation

Current tails during depolarizations to voltages near the i_f half-activation range display a time course that is well approximated by a single exponential, as seen in Fig. 4. On larger depolarizations, on the other hand, at voltages positive to the half-activation range, it cannot be excluded that the current tails have a more

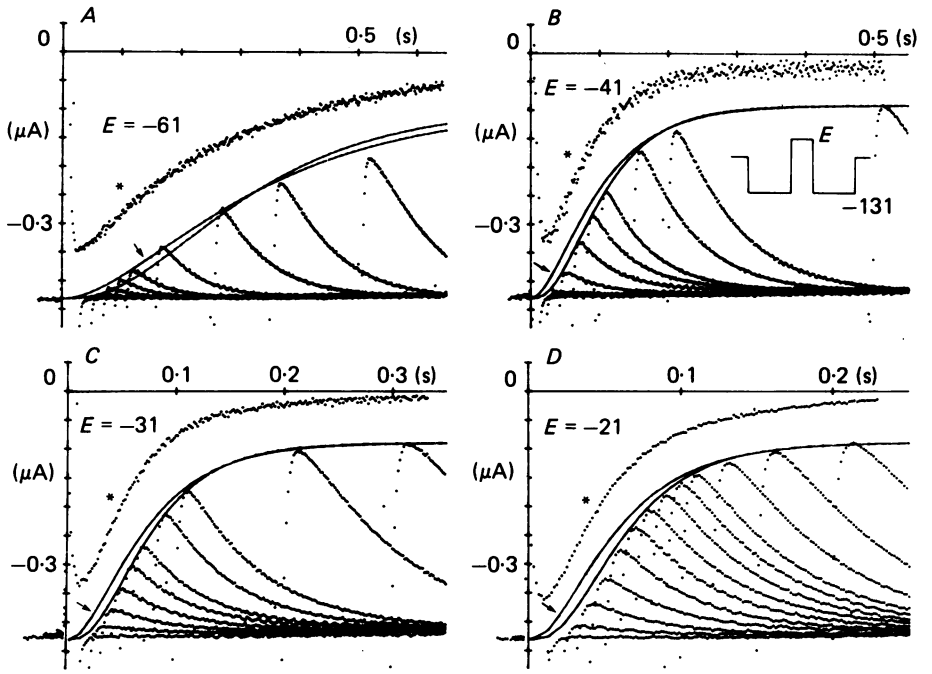

Fig. 5. Envelope tests at −61 (*A*), −41 (*B*), −31 (*C*) and −21 mV (*D*). The voltage protocol is shown in the inset in *B*. The current was activated with a 600 ms pulse to −131 mV and then deactivated by pulsing to the test potential *E* for various durations. The time development of deactivation was then revealed by applying a third pulse to −131 mV. The envelope refers to the traces recorded during this third pulse. Above each set of curves, for direct comparison with the corresponding envelopes, current tails during deactivation at the test potential *E* are also shown (asterisks). The tails have been scaled up to the current amplitude at −131 mV (340 nA) and their vertical position is arbitrary (notice that in *B*, *C* and *D* they are upside down, as the original current record is outward). Continuous lines in each panel represent fittings of envelopes with exponentials to a power of 2 (arrows) or 3.

complex, possibly sigmoid time dependence (see for example Fig. 2). However, a proper analysis of the i_f deactivation time dependence cannot be done by simple inspection as it can for current activation at large negative potentials, because of interference of residual onsetting inward transients (evident in Figs. 2, 5 and 9). To overcome this problem, envelope tests can be performed at potentials where inward transients are eliminated, as illustrated in Fig. 5. Each panel in Fig. 5 shows records

of i_f activation at a fixed potential of -131 mV after pulses to different voltage levels (-61 to -21 mV) of variable duration. The depolarizing pulses are all applied at the end of a 600 ms pulse to -131 mV given to activate i_f fully. It is obvious that, like activation, i_f deactivation too is S-shaped. This property becomes more pronounced at more positive potentials. The comparison between the envelope of i_f residual activation and the current deactivation in each panel of Fig. 5 shows that the sigmoid nature of the tail is not artifactual, and reflects a kinetic property of i_f. At the potentials of -41, -31 and -21 mV (panels *B*, *C* and *D* in Fig. 5) the time course of deactivation is well fitted by an exponential to the power $n = 3$, while a power of 2 is clearly insufficient (the presence of relatively large capacity transients makes the fit look worse than it probably is, particularly at -21 mV, panel *D*). At less positive levels (-61 mV in panel *A*) neither value gives a satisfactory fit, and the deactivation is characterized by a time course closer to a single exponential ($n = 1$), although an S-shape is still apparent. The consequences of a sigmoid decay are discussed later (see Part II of Results).

Modification of the time course of i_f activation by hyperpolarizing pre-pulses

Fig. 6 shows current records during pulses to -105 (*A*) and -115 mV (*B*) from a holding potential of -35 mV (traces labelled 'c' in each panel), and during pulses to the same voltages after pre-hyperpolarizations of various durations to -155 mV. Pre-hyperpolarizing causes the current traces to shift to the left on the time axis, as though a 'delay' in current activation were removed. Prolonging the pre-pulse duration makes the current activation less sigmoidal, until a single exponential time course is observed (see middle panels). In the lower panels of Fig. 6 the traces have been shifted on the time axis until the late part coincides with the control record. Superposition appears to occur for short pre-pulse durations, but durations longer than 8 ms induce an apparent acceleration with respect to control. This is also evident from the middle panels, where the traces are plotted on a semilogarithmic scale, and where records corresponding to the longest pre-pulse durations (lowermost traces) have a time dependence visibly faster than single exponential. The phenomenon observed in Fig. 6 cannot be directly compared with that seen for K^+ currents in nerve tissues, where hyperpolarizing pre-pulses induce a prolongation of the activation delay (see for example Begenisich, 1979). Indeed, in any Hodgkin–Huxley model with several gating subunits, pre-pulses that trigger a partial current activation (e.g. in the hyperpolarizing direction for the case of i_f) are expected to produce a 'shift' of the subsequent current activating record on the time axis. Thus a phenomenon comparable to that seen in nerve tissues for K^+ currents would be one where pre-depolarizations induced longer activation delays in i_f. This, however, was not observed. That is, when pre-depolarizing pulses of amplitudes and durations comparable to those of the hyperpolarizing pre-pulses in Fig. 6 were applied, no significant change in the following current development was observed (not shown). The data in Fig. 6 do, however, contain information that bears on a proper choice of kinetic model for i_f. Indeed, as for K^+ currents in the squid axon (Clay & Shlesinger, 1982) and myelinated nerve (Begenisich, 1979), traces corresponding to different pre-pulses in Fig. 6 do not always superimpose after time shift. This property is not compatible with Hodgkin–Huxley systems composed of identical, independent subunits (Hill & Chen, 1971; DiFrancesco & Ferroni, 1983).

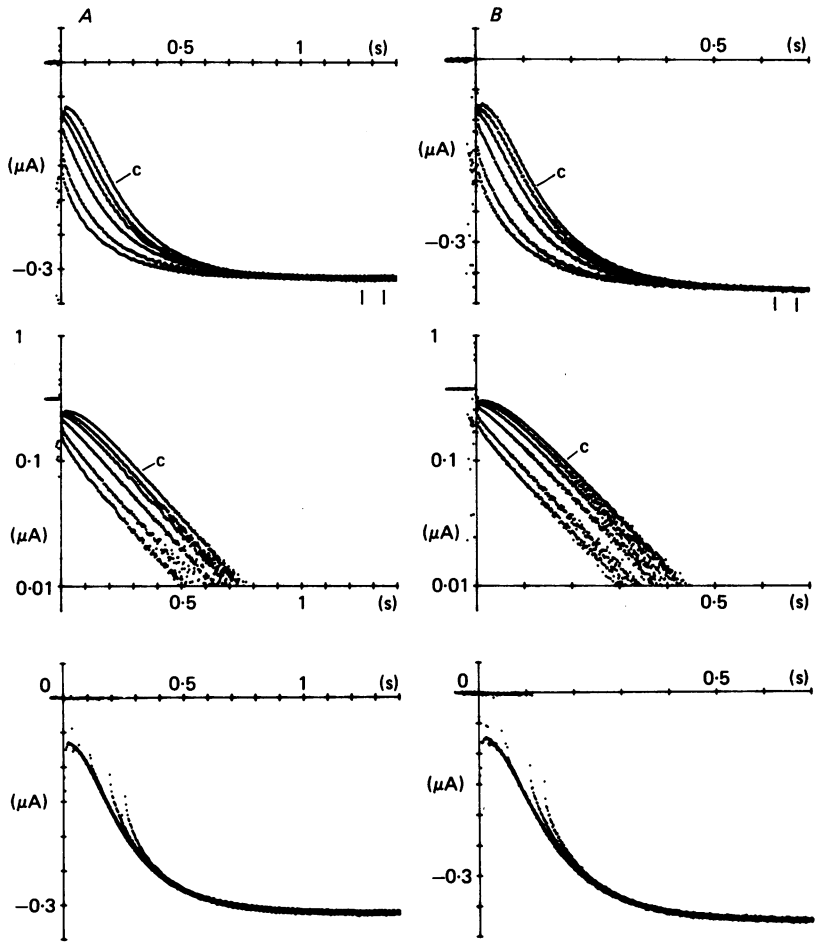

Fig. 6. Upper panels: current activation on pulsing to −105 (*A*) and −115 mV (*B*) from a holding potential of −35 mV (traces marked 'c') and after pre-hyperpolarizations to −155 mV for 2, 4, 8, 14 and 18 ms (*A*) and 2, 4, 8, 14 and 16 ms (*B*) (traces progressively displaced to the left). Middle panels: curves plotted on semilogarithmic scale. Lower panels: same records after shifts on the time axis of 27, 52, 95, 170, 250 ms (*A*) and of 15, 31, 56, 105, 135 ms (*B*) respectively for the 2–18 ms pre-pulses (*A*) and the 2–16 ms pre-pulses (*B*).

Repriming of the 'delaying' process

Having excluded the possibility that i_f activation occurs according to Hodgkin–Huxley models, even with several independent subunits, the simplest interpretation of the data of Fig. 6 would suggest the presence of a 'delaying' process that takes place before an otherwise faster activation (faster than a single exponential) takes over. The time required to remove the 'delay' at a given potential can be roughly estimated from experiments like those in Fig. 6 as the duration of the pre-pulse which is necessary to make the current activate according to a single exponential during the following test pulse, without greatly reducing its amplitude. For example, in the case of Fig. 6 a pulse to −155 mV of about 8 ms duration is sufficient to remove the

delay in the current activation at −105 and −115 mV. Repriming of this hypothetical 'delaying' process can be studied with experiments like those shown in Fig. 7. A test activating pulse to −133 mV is here preceded by two pulses, one of short, fixed duration to a voltage level at which a large fraction of delay is removed from the test activation record (see Fig. 6), and one of variable duration to a more depolarized level. The time required for the current trace to reach an apparently steady 'delayed'

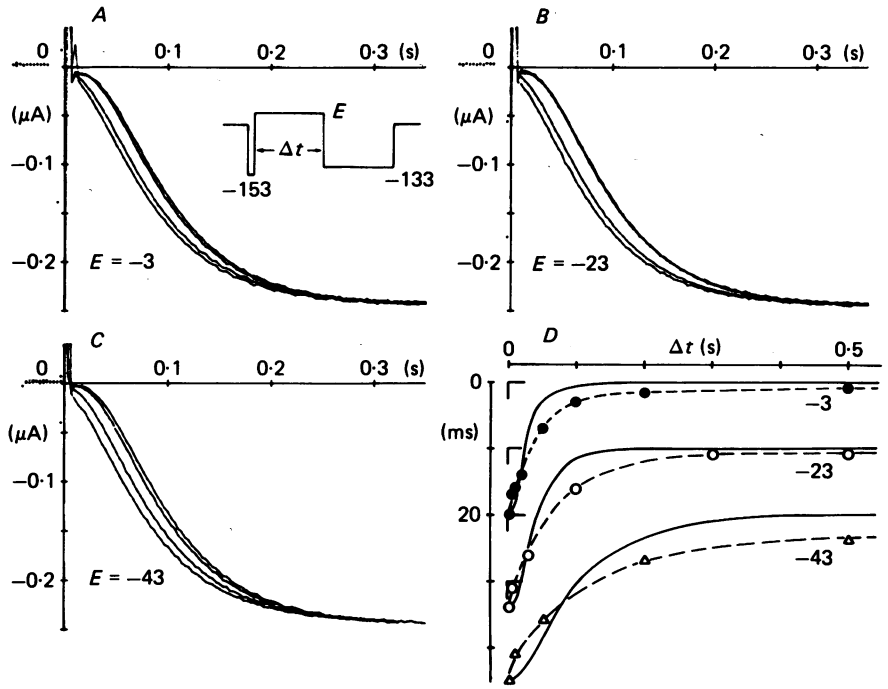

Fig. 7. 'Delay' repriming. After a pre-hyperpolarization to −153 mV for 10 ms, applied to reduce the delay in a subsequent activation, the membrane is held at a given potential (−3 (*A*), −23 (*B*) or −43 mV (*C*)) for a variable time, Δt, in the range 2–5000 ms, before a test activating pulse to −133 mV is applied (see inset). The traces shown correspond to pulses to −133 mV. From left to right in each panel four traces are shown corresponding to Δt = 2, 20, 100, 1000 ms (*A*); Δt = 2, 30, 500, 3000 ms (*B*); Δt = 2, 50, 500, 5000 ms (*C*). In *B* the third and fourth traces are practically coincident. *D*, dependence of the delay on Δt. The time shift required for superimposition with a reference trace (taken as the right-hand trace in each panel) is plotted against the duration Δt of the corresponding depolarizing pulse. The vertical scale refers to the −3 mV curve (●) while the −23 (○) and −43 mV (△) curves have been shifted by 10 ms for clarity. Also drawn in scale for comparison are curves measured as in Fig. 5 from envelope tests at the same potentials (continuous lines).

configuration during the test pulse gives an indication of the repriming time for a hypothetical delaying process. The curves plotted in Fig. 7*D* (dashed lines) show that this time is shorter at more positive potentials. Half-times range from about 35 ms at −3 mV to about 90 ms at −43 mV in the present experiment. It is important to observe that although this half-time is comparable to that of current deactivation at the same potential, the time courses of delay repriming (dashed lines) and of current deactivation (continuous lines in Fig. 7*D*) at the same potential are quite

dissimilar. The current deactivation curves are deduced from envelope test protocols as shown in Fig. 5, and their amplitude has been scaled up to the amplitude of the corresponding delay repriming curves for direct comparison. This is in contrast with the view that the two processes (channel closing and delay repriming) are linked, and favours the hypothesis that some degree of co-operativity among the gating subunits exists. This problem will be treated later in Part II of Results, where a channel model for i_f kinetics is proposed.

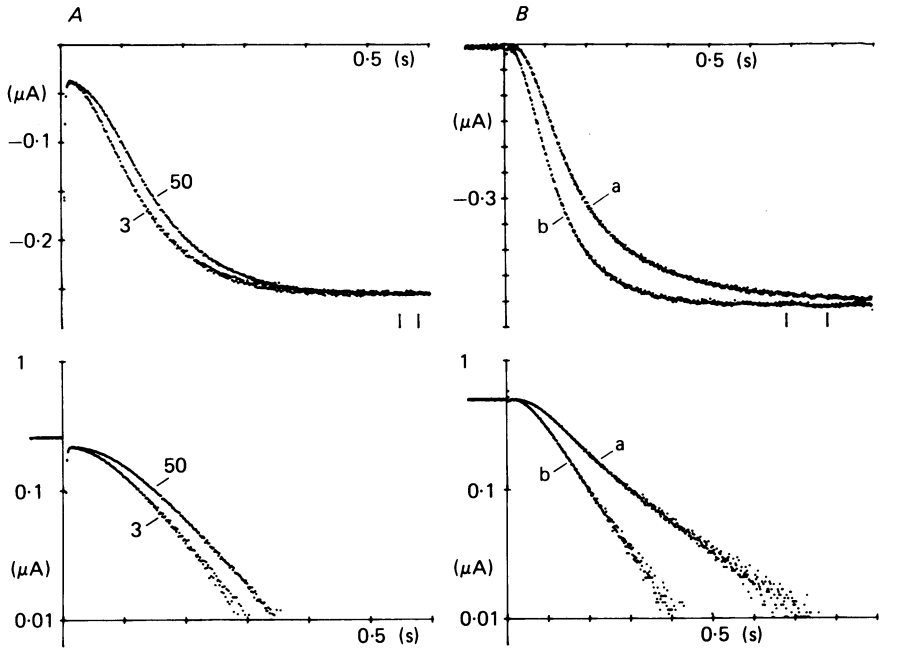

Fig. 8. *A*, trains of 700 ms pulses to −123 mV at different frequencies are applied from a holding potential of −33 mV. Traces corresponding to cycle times of 3 and 50 s are shown. *B*, a different fibre: current recorded during the first (a) and the second (b) pulse to −130 mV from a holding potential of −50 mV in a train where the cycle time was 5 s. From the semilogarithmic plot in the lower panel a large difference in the 'delay' time is not evident. Later pulses in the train elicited records perfectly overlapping the second pulse record (b).

Slow time-dependent changes in current kinetics

The data of experiments like those shown in Fig. 7 indicate that the apparent 'delay' in current activation can be restored after times of the order of 300–1000 ms in the voltage range −43 to −3 mV. Increasing the depolarized pulse duration up to 5 s does not seem to alter the current time course significantly during a subsequent activating hyperpolarization, as implicit in the flattening of the delay-duration curves in Fig. 7*D*. This would thus imply that the 'delay repriming' process has saturated. However, holding the depolarized voltage level for much longer times (of the order of minutes) causes the current time course to change further. Rather than being a further increase in the apparent activation delay, however, this change appears as a slowing down of the activation process. Fig. 8 shows this phenomenon in two experiments where the protocols were simpler than that of Fig. 7, and consisted in

applying trains of activating pulses with different cycle times (*A*), or trains of pulses at a given frequency after a long rest period (*B*). Comparing the current activation time course corresponding to the shorter (3 s) with that corresponding to the longer (50 s) cycle time in *A*, or the current time course of the first (a) with that of the second (b) activating pulse (in a train given after a 2 min rest interval) in *B* shows that long rest periods at depolarized potentials cause a sometimes very noticeable slowing down of the channel opening process. In experiments like the one in Fig. 8*B*, the current record during the third and the following pulses remains unchanged, also indicating

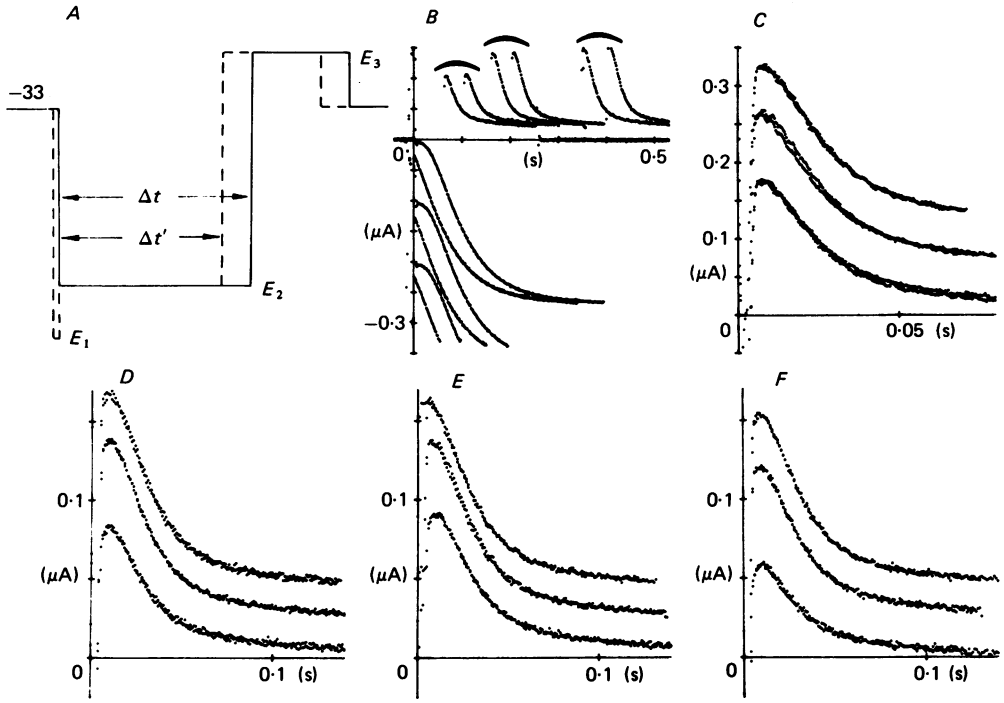

Fig. 9. Time course of deactivation after delayed or non-delayed activation. *A*, voltage protocol used. Pairs of hyperpolarizing pulses to E_2 (with or without a negative pre-pulse to E_1) are applied before a test deactivating pulse to E_3. The duration Δt of the pulse to E_2 is previously fixed, and the duration $\Delta t'$ of the companion pulse preceded by the pre-pulse to E_1 is then selected to yield the same final value of current. *B*, examples of traces recorded with $E_1 = -163$, $E_2 = -133$ and $E_3 = -13$ mV. The values of Δt were 100, 200 and 400 ms (activation records corresponding to $\Delta t = 100$ and 200 ms have been shifted downwards for clarity). *C–F*, sets of pairs of records during pulses to E_3. In all panels except *D*, Δt was 200, 400 and 600 ms respectively for the lower, middle and upper pair (in *D* 100, 200 and 400 ms were used). Values of E_1, E_2 and E_3 were (in mV): *C*, −123, −3 and −153; *D*, −133, −13 and −163; *E*, −123, −13 and −153; *F*, −113, −13 and −143 mV. In all cases superimposition of records in a pair is nearly perfect.

that the process associated with the observed change requires times of the order of several seconds (indeed, minutes) to develop. The slowing down caused by long rest periods is not altered if in Fig. 8*B* the current deactivation is accelerated by depolarizing to more positive levels (−30 to 10 mV for 400 ms) after the negative pulses, implying that this process is totally independent from channel closing (not

shown). These facts, together with the observation that the change induced by prolonging the holding potential duration is not a simple time shift, but a slowing down of the activating process, indicate that this phenomenon is different from the one observed previously in Fig. 7. Phenomena which occur at this low speed are more likely to be associated with processes involving changes of ion concentrations near the membrane than with true channel kinetics. The possible causes of the phenomenon seen in Fig. 8 have not been investigated in the present paper for two main reasons: first, the process giving rise to the change in the current time course seen in Fig. 8 is probably attributable to processes other than current kinetics, and secondly, even if this were the case it is difficult to see the physiological relevance of a process requiring times of the order of minutes to produce significant changes in the current kinetics. Thus, this study has been restricted to changes in the current kinetics involving times that are within the physiological range.

Independence of channel deactivation from the 'delaying' process

The data in Fig. 7 show that, as for half-times of i_f deactivation (Hart, 1983), the time required for full delay repriming decreases at more positive potentials. The time course of delay repriming shown in Fig. 7*D* is, however, evidently different from the time course of i_f deactivation at the same potential. The former process is not apparently S-shaped, and takes longer to saturate than the latter. This favours the view that the two processes are independent from each other. To investigate this aspect more fully, experiments like those shown in Fig. 9 can be performed. Here the current decay after partial activation at a given voltage is compared with that obtained with the activating pulse preceded by a conditioning pre-hyperpolarization. In the latter protocol, the activating pulse lasts long enough to bring i_f to the same value as in the absence of the pre-pulse. Pairs of current tails corresponding to different activating and/or deactivating voltages are compared in Fig. 9*C–F*. It appears that, with a relatively high degree of accuracy, the time course of i_f deactivation depends not on the degree of 'delay' present but only on the initial current value. These data suggest that the 'delaying' and 'closing' processes occur independently from each other.

Part II. Modelling of i_f kinetics

This section is devoted to the comparison of experimental data shown in Part I with the predictions of channel kinetic schemes, with the aim of selecting a suitable representation of the observed properties of i_f. As quoted in the Appendix, the selection is done on models where the channels are considered as independent and identical entities, composed of a given number of generally non-identical, non-independent gating subunits, each of which is supposed to have only two states. The need for investigating models with non-identical and/or co-operating subunits is a straightforward deduction from the data presented in the experimental part of this paper. Indeed, as shown in Part I above, Hodgkin–Huxley models fail to explain essential features of i_f kinetics. Thus, more complex kinetics are necessary. The construction of a suitable model for i_f kinetics must obviously start from the consideration of the current properties as revealed by the experiments shown in the previous part of this paper. Thus, for example, it will be necessary to explain how

the current activation, normally sigmoidal, can be made to follow a single-exponential time course without apparent delay after a given pre-hyperpolarization (Fig. 6), and how, on the other hand, current deactivation is S-shaped, too (Fig. 5). The simplest way to account for the S-shaped current activation normally observed is to assume that a retarding process takes place before the actual opening can occur. A reaction scheme illustrating this assumption is shown in Fig. 10. Here, two 'delaying' subunits

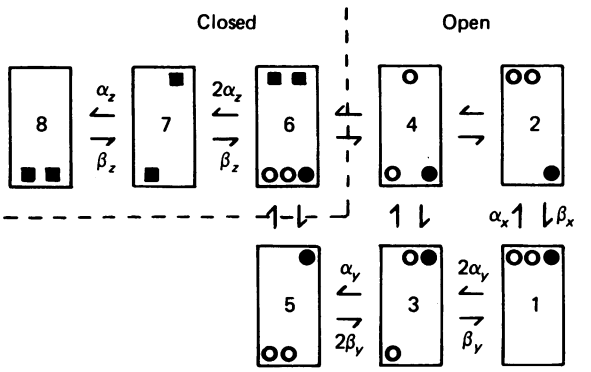

Fig. 10. Kinetic scheme used to fit the experimental data. Each rectangle represents a distinct channel configuration. Channel subunits are of three different types: x (single, ●), y (double, ○) and z (double, ■). Open configurations are 1–5, and closed configurations 6–8. The 'gating' subunits x and y occupy bottom positions in all closed configurations and for simplicity have not been drawn in 7 and 8. The 'delaying' subunits z occupy the top position in 6 and in all open configurations 1–5, and have been dropped in the latter. Twin configurations have been accounted for by doubling the rate constants where appropriate. The fully open configuration 1 corresponds to all subunits in the top position (values: x, y and z), while the fully closed configuration 8 corresponds to all subunits in the bottom position (values: $1-x$, $1-y$ and $1-z$).

(z) need to be in a given state (state 6) before the gating process, through the subunits x and y, takes place during a negative pulse. This reaction scheme incorporates all the essential features of i_f kinetics as derived from the experimental results shown in the previous section. These are as follows.

1. Presence of several open (1–5) and closed (6–8) channel configurations. According to the convention adopted in the Appendix, in this scheme the fully open and fully closed channel configurations, corresponding to extreme negative and extreme positive potentials, are 1 and 8, respectively. There is evidently no direct transition from the fully closed (fully open) state to any open (closed) configurations. As shown in the Appendix, this is required as a general condition to reproduce both sigmoidal activation and deactivation as experimentally observed.

2. Third power for both activation and deactivation. The data in Fig. 5 show that a power of at least 3 is needed to fit the time course of deactivation at potentials positive to −40 mV. Thus, three independent subunits (x and y) have been included to preside over the actual 'gating' processes in the scheme of Fig. 10. A similar reasoning applies to the choice of two z subunits in relation to the data in Fig. 3.

3. Approximately single-exponential behaviour during deactivation at potentials in the middle of the activation range. This property, illustrated in Fig. 4, can be reproduced by using two gating subunits of one type (y) and one of a different type

(x). A single-exponential current decay is thus obtained, assuming that x changes much more slowly than y during depolarizations to the middle region of the activation range (around $-70/-80$ mV).

4. Non-interference of the delaying process with channel closing. This is not a strict requirement but it is suggested by the lack of evidence of interaction between the two processes (Fig. 9). It is simply obtained by letting the z subunit move within the set of closed channel configurations only (6, 7 and 8 in the scheme of Fig. 10).

Reconstruction of the current time course during voltage-clamp pulses

The aim of the model outlined above is the reproduction of the voltage-clamp data reported in the experimental part of this paper. The reaction scheme used (Fig. 10) is complex enough to make a numerical solution preferable to an analytical one. The method used to integrate the relevant kinetic equations is explained in the Appendix and in the Methods section.

The ability of the scheme in Fig. 10 to fit experimental records during pulses from holding potentials at either side of the i_f activation curve (termed f_∞), where channels can be assumed to be in one of the extreme configurations (1 or 8), and the initial conditions for the integration of eqn. (1) are easily determined, is illustrated in Fig. 11. Current traces during activation in the range -79 to -164 mV (A) and during deactivation in the range -29 to -9 mV (B) in the same fibre are shown together with the curves predicted by the model (open circles). Values of the time constants and activation fractions used in the fitting procedure, together with the measured f_∞ curve, are shown in Fig. 14 A below. The model clearly reproduces both the sigmoid activation and deactivation. Panels C and D show in another fibre the fitting of deactivation at two potentials, -61 (C) and -21 mV (D), where envelope tests were performed to improve the resolution of the deactivation time course. The experimental records are the same as those shown in Fig. 5. Again, the model predictions are satisfactory if compared with those obtained with Hodgkin–Huxley models in Fig. 5. Reproducibility of data from pre-pulse experiments like those in Fig. 6 is tested in Fig. 12. Pulses to the range -94 to -124 mV are preceded by pre-pulses in the range -134 to -164 mV for variable durations (5–30 ms). For each panel, all theoretical curves (open circles) were computed with the same steady-state parameters but different initial conditions (that is, with different initial probability vectors). The latter were obtained by running the computation of the theoretical curve fitting the proper hyperpolarizing pre-pulse trace for a time corresponding to the experimental pre-pulse duration. It is worth noticing that with this procedure no free parameter can be adjusted once the test (no pre-pulse) and the pre-pulse records have been fitted. Despite this restriction, the model describes satisfactorily the changes induced by conditioning negative pre-pulses on the time course of activation, although it fails to reproduce entirely the acceleration caused by particularly long pre-pulses (lowermost traces in panels A, B and C of Fig. 12). In the same experiment four more sets of curves at different potentials were recorded and analysed with similar results.

Fitting of a full set of data in a single experiment permits a fuller reconstruction of the voltage dependence of activation variables and time constants. Figs. 13 and 14 report the results of an experiment where activation (13 A) and deactivation (13 B) of i_f were studied in the voltage range -13 to -153 mV, together with the properties

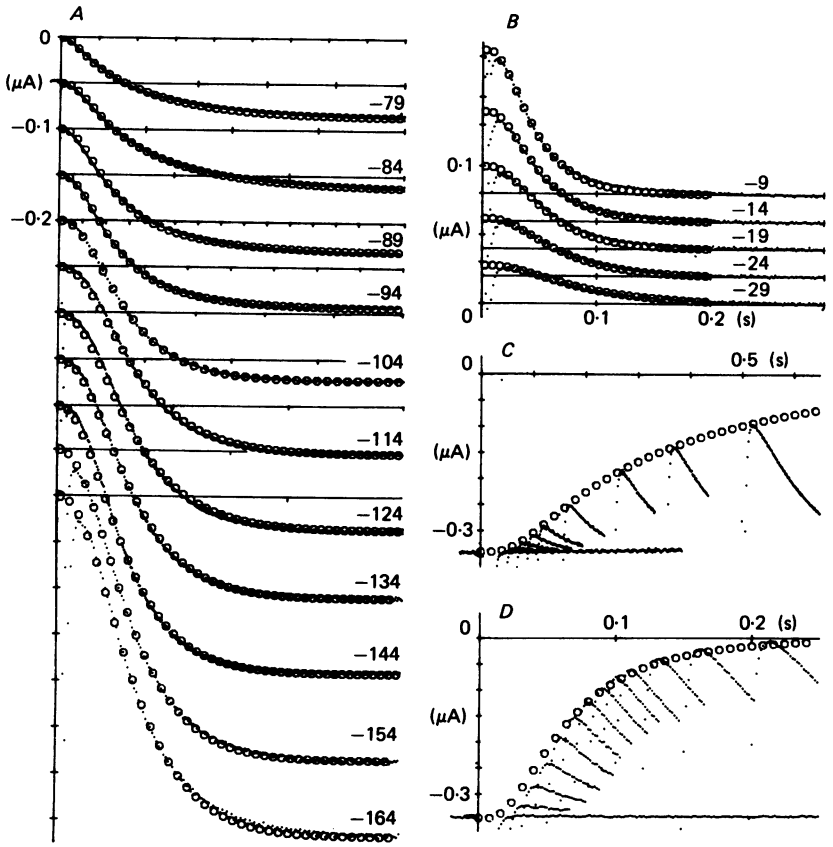

Fig. 11. Fitting of current activation and deactivation time course. *A*, current activation in the range −79 to −164 mV. Holding potential was −34 mV. *B*, deactivation during pulses to the range −29 to −9 mV following activation at −124 mV for 800 ms. Traces shifted vertically for clarity. Theoretical curves are indicated by open circles. In *A* each trace has a different time scale (the unit is either 1 s for the first four traces, or 0·1 s). All the parameters used to fit the records in *A* and *B*, including the steady-state probabilities before pulsing, and excluding the steady-state current value at each potential, are plotted in Fig. 14*A*. *C* and *D*, same experiment as in Fig. 5. Model fitting of current deactivation measured with envelope tests at −21 (*C*) and −61 mV (*D*). Values of parameters used to fit the envelopes are reported in Fig. 14*B*, and coincide with those used to fit the deactivation records at the corresponding potentials in the same experiment.

of the delaying process (13*C*, *D*). Also shown in Fig. 13, to the right of each corresponding set of experimental curves, are the curves predicted by the model in Fig. 10. The voltage dependence of time constants and activation variables at steady state used to fit these results is shown in Fig. 14*C*, together with the experimental f_∞ curve. Fitting of activation and deactivation records is satisfactory. Moderate and pronounced S-shaped time courses of both onset and decay at potentials around −80 mV and out of this range, respectively, are well reproduced. Indeed the presence of a relatively slow component on activation during small negative pulses is also at least to some extent reproduced (see for example the trace at −93 mV). Thus, results like those shown in Fig. 4, where activation and deactivation at the same voltage

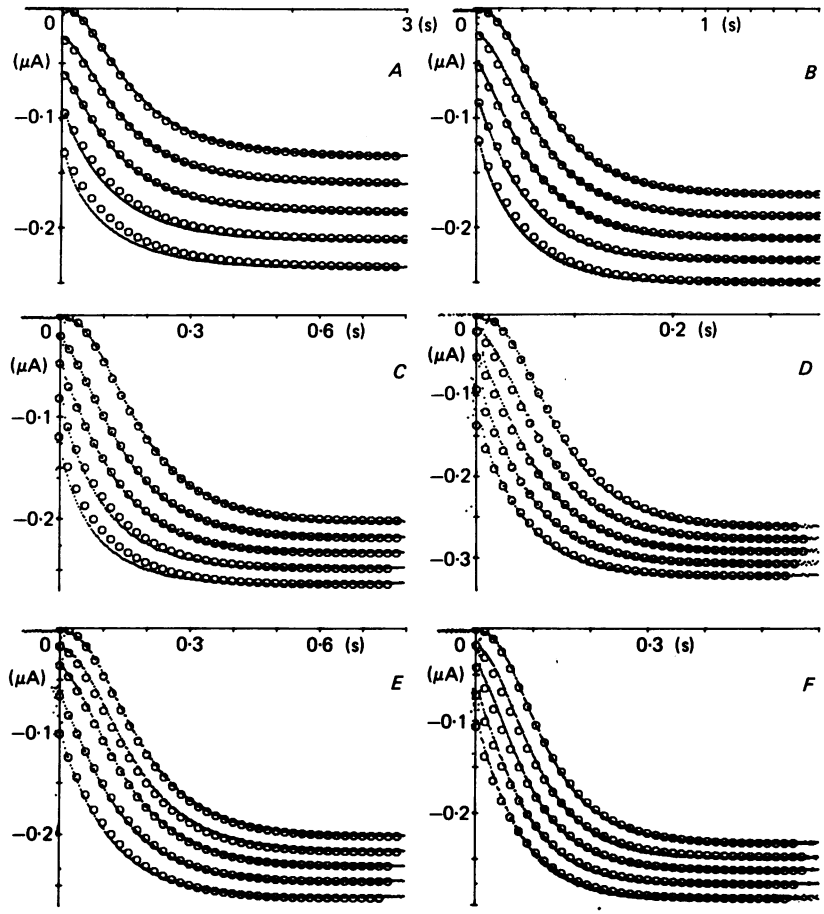

Fig. 12. Fitting of data from experimental protocols as in Fig. 6. Same experiment as in Figs. 2 and 11 *A*, *B*. Pre-pulses and test pulses were to the following voltages (in mV): *A*, −154 and −94; *B*, −154 and −104; *C*, −164 and −114; *D*, −164 and −134; *E*, −144 and −114; and *F*, −154 and −124. Pre-pulse durations were 5, 10, 15 and 20 ms in all cases except in *E*, where they were 5, 10, 20 and 30 ms. In all panels records corresponding to increasing pre-pulse durations are shifted downwards by fixed amounts. Theoretical curves, indicated by open circles, were computed by using the parameters plotted in Fig. 14 *A*. All records in each panel fitted with the same parameters. Fitting of curves at −144, −154 and −164 mV used to compute initial probability vectors for each record following a pre-pulse is shown in Fig. 11 *A* (three bottom traces).

level are shown to differ in their time courses, can also be accounted for by the model (see pulses to −78, −83 and −88 mV). Removal of the activation delay (panel *C*) is also well described. The reconstruction of the traces recorded on an envelope test during depolarizations (panel *D*) is less satisfactory in both the onset of current reactivation and the delay recovery, although both processes are obviously qualitatively accounted for.

The theoretical curves of Fig. 14 provide the essential features that the reacting subunits x, y and z in the scheme of Fig. 10 need to have in order for the same scheme to be applicable to i_f kinetics. First, the relative position of the activation curves is

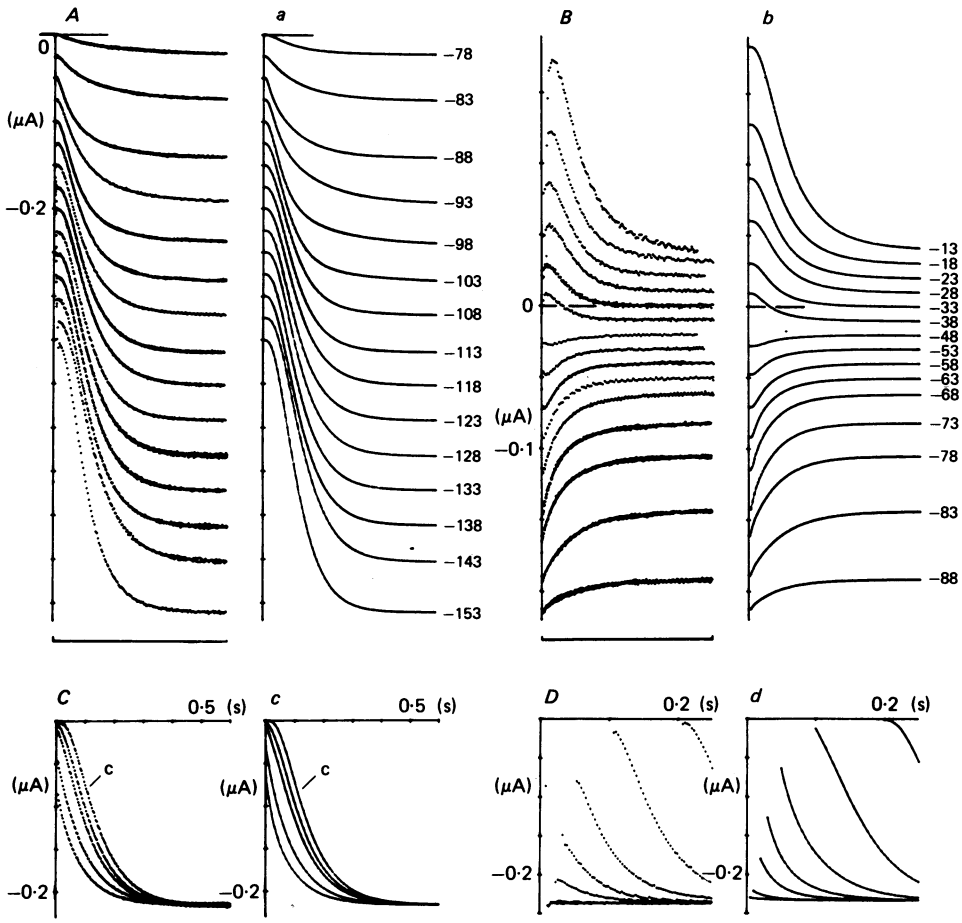

Fig. 13. Comparison between experimental data (*A–D*) and model predictions (*a–d*). The experiment was the same as in Figs. 7 and 9. In all panels the vertical scale unit is 50 nA. *A* and *a*, current activation in the range −78 to −153 mV. For top to bottom traces respectively the horizontal bar is (in s): 15, 15, 15, 7, 5, 3, 2, 1·2, 1, 0·7, 0·6, 0·5, 0·4, 0·3 and 0·25. From top, traces shifted vertically by −25 nA each. *B* and *b*, current deactivation in the range −88 to −13 mV, recorded following a 700 ms pulse to −133 mV. The horizontal bar is (top to bottom, in s): 0·15, 0·18, 0·2, 0·22, 0·32, 0·4, 0·8, 1·2, 1·8, 3, 5, 10, 15, 15 and 15. Traces shifted by 10 nA with respect to each other. *C* and *c*, the test pulse (trace 'c') was to −123 mV and was preceded by 5, 10, 20 and 30 ms pulses to −153 mV. The parameters used to fit the pre-pulse-induced change of initial conditions were those giving the fit for the −153 mV record in panel *a*. The computation was performed as explained in Fig. 12. Similar results obtained at −113 and −133 mV. *D* and *d*, records from an envelope test at −23 mV. Pulses of various durations (5, 10, 20, 30, 50, 100 and 200 ms) to −23 mV were preceded and followed by a 400 ms pulse to −133 mV. As in *c*, no free parameter was used in these computations. Similar results obtained for envelope tests at −33 and −13 mV.

such that the $f_\infty(E)$ curve nearly coincides with the $x_\infty(E)$ curve. Secondly, time constants for the x subunit are much larger than those for y, particularly close to the half-activation range, and the peak voltage for τ_x is more positive than that of τ_y. This is consistent with the relative positions of the corresponding activation

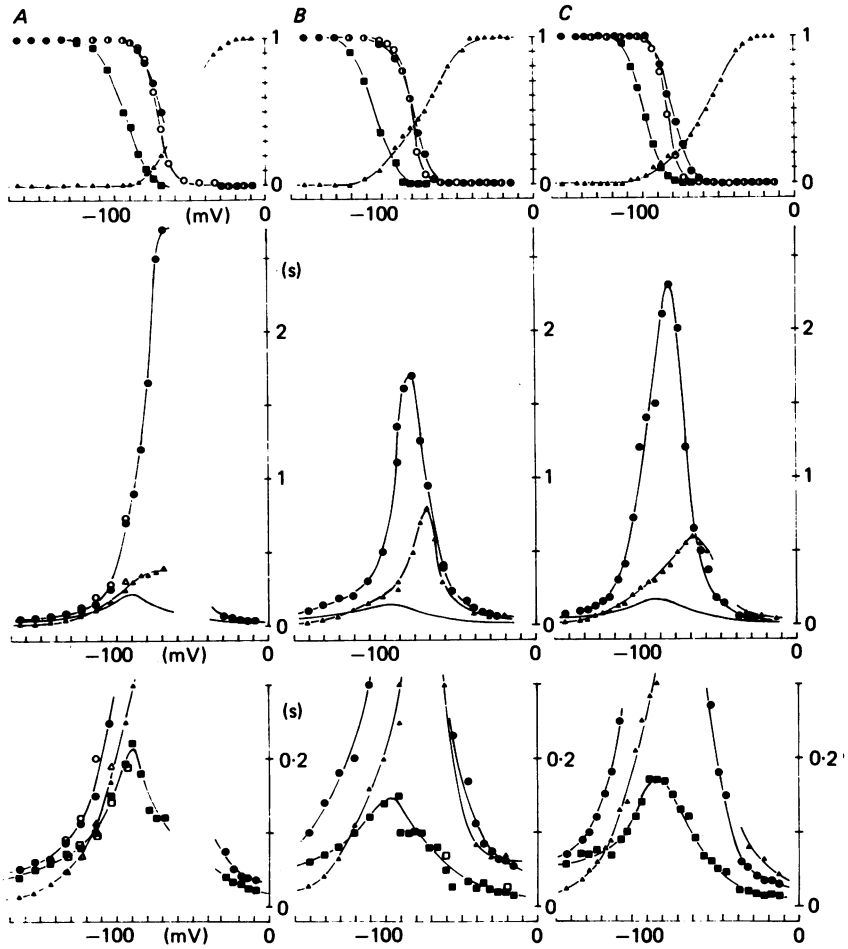

Fig. 14. Voltage dependence of kinetic parameters evaluated by data fitting from different protocols in three experiments. Plots in *A*, *B* and *C* refer to the experiments in Figs. 11*A* and 12, in Fig. 11*B*, *C* and in Fig. 13 respectively. Upper panels: values of the steady-state activation fractions x_∞ (●), y_∞ (■) and $1-z_\infty$ (▲) (shown instead of z_∞ to improve clarity). The experimental f_∞ curves are also shown (○). Middle and lower panels: time constants τ_x (●), τ_y (■) and τ_z (▲) plotted on two different scales for better resolution. The values reported with open symbols were obtained by fitting of records from two- or three-pulse protocols as shown in Figs. 12 and 13*C*, *D*. For clarity, only continuous lines drawn by eye to fit the τ_y curves are shown in the middle panels.

curves. The τ_z curve appears to be slightly more displaced to the right, although the precise position cannot be determined on the basis of single deactivation records, because the current decay does not depend on the 'delaying' subunit z, at least during relatively large depolarizations. This, as noted above, is one of the properties of the reaction scheme in Fig. 10, and is consistent with the results of Figs. 7 and 9. Some indication of the values of τ_z at depolarized voltages (panels *B* and *C* of Fig. 14) is given by fitting of experiments where the delay recovery can be studied, as in Fig. 11*C*, *D*.

DISCUSSION

Since the original study of the axonal currents by Hodgkin & Huxley (1952), sigmoidal activation has been described for K^+, Na^+ and Ca^{2+} currents in various tissues (myelinated nerve: Frankenhaeuser, 1963; Hille, 1973; Dubois, 1981; lobster nerve: Julian, Moore & Goldman, 1962; skeletal muscle: Adrian, Chandler & Hodgkin, 1970; Adrian & Peachey, 1973; for Ca^{2+} currents see Hagiwara & Byerly, 1981). According to Hodgkin–Huxley type models, activation is retarded by the contribution to the opening process of several identical and non-cooperating gating subunits in a kinetic scheme where the channel is assumed to be open when *all* subunits are in a given state. Such models have been widely used to explain current kinetics in different excitable tissues, and only recently has their validity been discussed in relation to experiments where, as in Fig. 6 of this paper, the effects of conditioning pre-pulses on current activation are considered. In myelinated axons (Begenisich, 1979) and in squid axons (Clay & Shlesinger, 1982), for example, when K^+ current activation is preceded by a negative pre-pulse, the current time course cannot be made to superimpose on that in the absence of a pre-pulse, a property unexplained by Hodgkin–Huxley models. This behaviour can be used to support the view that co-operativity exists among subunits (Hill & Chen, 1971), although other explanations are possible.

In the heart, Hodgkin–Huxley type models have been used to fit Na^+, K^+ and Ca^{2+} currents, and the electrical activity of cardiac tissues has been successfully reconstructed using such models (McAllister *et al.* 1975; Beeler & Reuter, 1977; D. DiFrancesco & D. Noble, 1984, unpublished observations; H. F. Brown, J. Kimura, D. Noble, S. J. Noble & A. Taupignon, 1984, unpublished observations). In the original interpretation, the cardiac pace-maker current kinetics were described in terms of a single Hodgkin–Huxley activation parameter, in agreement with the observation that current activation and deactivation followed single-exponential time courses (Noble & Tsien, 1968). Indeed, as shown in Fig. 4, a single exponential can be used to approximate the current time dependence for both onset and decay near the middle of the activation curve, a range where measurements done in the presence of substantial K^+ accumulation/depletion phenomena are possibly more reliable than elsewhere.

In a recent study of i_f kinetics in sheep Purkinje fibres in the presence of Ba^{2+}, Hart (1983) reports a delayed development of i_f activation during a hyperpolarization. The data presented here show that the S-shaped i_f activation is not an artifact, but a genuine property of this current system. In Ba^{2+}, the Cs^+-dependent current is nil at holding potentials of near -40 mV and at the start of voltage-clamp hyperpolarizations down to -130 mV (Fig. 3), indicating the complete absence of background Cs^+-dependent components such as i_{K1}. The use of Cs^+ also helps to reduce capacity transients and allows a specific pharmacological dissection of i_f, whose time course is then visibly sigmoidal. A similar dissection is possible as far as both the time-independent and capacity components during hyperpolarizations behave linearly with voltage, by using electronic subtraction procedures as illustrated in Methods. These procedures also lead to S-shaped current activation (Figs. 1, 7, 8*B*, 9 and 13). A further, more conclusive piece of evidence supporting the view that

the sigmoid nature of i_f is not artifactual comes from experiments where envelope tests are performed (Fig. 2). While the sigmoid activation of i_f could be accommodated in the framework of a Hodgkin–Huxley model simply by raising the power of its activation variable, several other aspects of i_f kinetics are not compatible with such a scheme. For example, envelope tests during current deactivation show that channel closing is also an S-shaped function of time (Fig. 5). As shown in the Appendix, this behaviour is explained by assuming the presence of several open configurations. Thus the data discussed above require a channel model where 'open' and 'closed' configurations are not unique. Furthermore, the i_f time course during activation at potentials close to the middle of its activation range approaches a single exponential, in contrast with the predictions of a multi-subunit Hodgkin–Huxley channel. The fact that activation traces with and without a conditioning pre-hyperpolarization will not superimpose (Fig. 6) puts further restrictions on the model of i_f kinetics. According to Hill & Chen (1971), superimposition is obtained if transitional states reached by the system are all 'equilibrium' states, a condition satisfied with Hodgkin–Huxley models. Clearly then, the data in Fig. 6 require a co-operative model (Begenisich, 1979), or a model with independent, but not identical gating subunits (this last condition also ensures that the states reached by the system are not necessarily equilibrium states). The observation that the delaying process influences channel opening, but not channel closing (Fig. 9), favours the view that the particles are not all independent, and some degree of co-operativity exists. Indeed, with independent models the situation where any one subunit takes part in the opening, but not in the closing process (or vice versa) cannot be reproduced.

Modelling of i_f kinetics

The attempt at reproducing i_f kinetics has necessarily to be based upon the observed current behaviour. The requirements to be fulfilled are the following.

1. At voltages out of the half-activation range the time course of both activation and deactivation should be fitted by exponentials to a power of at least 3.
2. The process inducing a delay in current activation should not affect channel closing.
3. The activation delay should be totally removed by preceding a test activating pulse by a suitable conditioning hyperpolarization. Application of a pre-pulse should be associated with acceleration of the activation time course.
4. Current deactivation should be well approximated by a single exponential near the half-activation range. The activation delay should be small in this range.

As reviewed in the Results section, the proposed scheme of Fig. 10, when proper values are assigned to the rate constants as functions of voltage, is able to satisfy the above requirements.

The criteria followed in developing the proposed model have been those of minimizing its complexity in relation to the data to be reproduced. It would obviously be possible to increase the complexity of that scheme (by for example increasing the number of subunits, or introducing finer degrees of co-operativity) for an improved data fitting. Several trials on less complex models, on the other hand, with a reduced number of gating subunits and/or of distinct configurations, have led to only partial fulfilment of the required properties. Reproducibility of experimental

data by the model is illustrated in Figs. 11–13, and can be considered as satisfactory. Fitting of the i_f kinetic behaviour deduced by single experiments in a more or less full range of voltages where i_f records are reliable gives a description of the properties of the x, y and z particles (Fig. 14). Activation of y subunits occurs at potentials more negative than for x and z subunits. This, together with the much larger values of τ_x with respect to τ_y, is necessary to explain the nearly single-exponential behaviour of i_f activation/deactivation at potentials around $-70/-80$ mV, and the more complex time dependence out of this range. Peak potentials in the time constant curves and half-activation potentials for the corresponding subunits appear correlated in Fig. 14, as expected in a self-consistent model.

Features of i_f kinetics unexplained by the proposed model

The model fails to mimic perfectly the very slow component present on hyperpolarizations in the half-activation range (Figs. 4 and 13). In some cases it also fails to reproduce quantitatively the acceleration induced by pre-pulsing on the current activation. Further complications in the model to accommodate these properties, as well as other properties not accounted for, like that shown in Fig. 8, have not been considered here because they are too speculative at the present stage.

Although the kinetic scheme explored here gives a reasonably good description of i_f kinetics and does satisfy the main requirements deduced from experimental data, it is difficult to assess how realistic this model is. This is, however, an intrinsic limitation of the presently available data, and of the limited amount of information that can be extracted from these data. It is likely that a variety of different kinetic models can describe the observed i_f behaviour equally well. As mentioned above, though, attempts to fit all the available data with simpler models have failed, essentially because at least one of the features of i_f kinetics could not be reproduced. In other words, the model of Fig. 10 incorporates in a relatively simple way all the features required to account for a whole set of experimental results. The model has in any case to be regarded as a descriptive one, and needs to be verified by experimental approaches other than the traditional voltage clamping.

APPENDIX

General solution for a system governed by first-order linear differential equations

Channel models considered here are those governed by the master equations:

$$dp_i/dt = \dot{p}_i = -\left(\sum_{j \neq i} k_{ij}\right) p_i + \sum_{j \neq i} (k_{ji} p_j) \quad i = 1, \ldots, n, \tag{A1}$$

where p_i is the probability that the system is in the ith state and k_{ij} is the rate constant for the transition i to j. The number of possible states is n. The set of eqns. (A1) can be reduced by one degree by substituting one of the probabilities (for example, p_n) using the relation

$$\sum_i p_i = 1. \tag{A2}$$

In matrix notation, the set of (independent) equations thus obtained is

$$A p + k = \dot{p} \tag{A3}$$

where

$$p = (p_1, p_2, p_3, \ldots, p_{n-1}) \tag{A4a}$$

$$k = (k_{n1}, k_{n2}, k_{n3}, \ldots, k_{n,n-1}) \tag{A4b}$$

and the matrix A is

$$A = \begin{bmatrix} -\left(\sum_{j\neq 1} k_{1j}\right) - k_{n1} & k_{21} - k_{n1} & k_{31} - k_{n1} \cdots & k_{n-1,1} - k_{n1} \\ k_{12} - k_{n2} & -\left(\sum_{j\neq 2} k_{2j}\right) - k_{n2} & k_{32} - k_{n2} \cdots & k_{n-1,2} - k_{n2} \\ \cdots & & & \\ k_{1,n-1} - k_{n,n-1} & k_{2,n-1} - k_{n,n-1} & k_{3,n-1} - k_{n,n-1} \cdots & -\left(\sum_{j\neq n-1} k_{n-1,j}\right) - k_{n,n-1} \end{bmatrix} \tag{A5}$$

Now the determinant of A is $\neq 0$, and eqn. (A3) can be rewritten as

$$A(p + A^{-1}k) = \frac{\mathrm{d}}{\mathrm{d}t}(p + A^{-1}k). \tag{A6}$$

With the initial condition $p = p_0$, the solution of (A6) is

$$p(t) = \mathrm{e}^{At}(p_0 + A^{-1}k) - A^{-1}k, \tag{A7}$$

where e^{At} is a matrix conventionally defined as the series

$$\mathrm{e}^{At} = I + At + \frac{(At)^2}{2!} + \frac{(At)^3}{3!} + \ldots, \tag{A8}$$

I being the identity matrix. It may be important to note that the elements of the matrix e^{At} do not in general have an exponential dependence on time. This only happens when A is a diagonal matrix. The steady-state probability vector is found by setting $\dot{p} = 0$ into eqn. (A3), which gives

$$p_\infty = -A^{-1}k. \tag{A9}$$

The time course of the probability vector can thus be written as

$$p(t) = \mathrm{e}^{At}(p_0 - p_\infty) + p_\infty. \tag{A10}$$

Eqns. (A9) and (A10) fully describe the kinetics of the system. Despite the compactness of the above formulation, however, calculation of the matrix e^{At} is often too complicated to allow an analytical solution of (A3). In these cases, a numerical solution is required. Channel models considered here have unique open/closed configurations in the limit of extreme negative/positive potentials (or vice versa). This is a consequence of selecting rate constants that are monotonic functions of voltage. These configurations, which are not necessarily the *only* ones corresponding to the open/closed channel states, will be referred to as 'fully' open/closed configurations. The fully open (closed) configuration is defined as state 1 (n) and the corresponding probability as $p_1(p_n)$. Each subunit is supposed to have only two stable states, and channels are assumed to be independent from each other.

Sigmoid activation/deactivation

Let the 'open' probability (p_{op}) be generally associated with the configurations 1 to r ($r < n$)

$$p_{op} = \sum_{i=1}^{r} p_i. \tag{A11}$$

Then, from (A1) and rearranging,

$$\dot{p}_{op} = \sum_{i=1}^{r} \dot{p}_i = \sum_{i=1}^{r} p_i\left(-\sum_{j=r+1}^{n} k_{ij}\right) + \sum_{i=r+1}^{n} p_i\left(\sum_{j=1}^{r} k_{ij}\right). \tag{A12}$$

Eqn. (A12) represents the master equation for the system subdivided into the two partitions containing configurations 1 to r and $(r+1)$ to n respectively. When this system relaxes starting from a fully open state, characterized by $p_1 = 1$, then

$$\dot{p}_{op}(t = 0) = -\sum_{j=r+1}^{n} k_{1j} \tag{A13}$$

and $\dot{p}_{op}(t = 0) = 0$ is only verified when

$$k_{1j} = 0 \quad j = r+1, \ldots, n. \tag{A14}$$

Thus, sigmoid relaxation from the fully open state (with zero time-derivative at $t = 0$) can only be obtained on condition that *there is no possible transition from the fully open to any closed configuration*. From eqn. (A12) it is readily shown that a similar condition applies to relaxations from the fully closed configuration (at which $p_n = 1$). According to (A12), therefore, delayed activation and deactivation will be present only if both the fully open and fully closed configurations have no *direct* link with closed and open states respectively.

The author is indebted to Drs H. F. Brown, G. Hart, D. Noble (Oxford), C. Bader, M. Bertrand (Geneva), A. Ferroni (Milan) and C. Ojeda (Lyon) for helpful discussions during this work and for exhaustive comments on the manuscript. Part of this work was supported by the C.N.R. (project no. CT 81.00648).

REFERENCES

ADRIAN, R. H., CHANDLER, W. K. & HODGKIN, A. L. (1970). Voltage clamp experiments in striated muscle fibres. *J. Physiol.* **208**, 607–644.

ADRIAN, R. H. & PEACHEY, L. D. (1973). Reconstruction of the action potential of frog sartorius muscle. *J. Physiol.* **235**, 103–131.

BEELER, G. W. & REUTER, H. (1977). Reconstruction of the action potential of ventricular myocardial fibres. *J. Physiol.* **268**, 177–210.

BEGENISICH, T. (1979). Conditioning hyperpolarization-induced delays in the potassium channels of myelinated nerve. *Biophys. J.* **27**. 257–266.

BEZANILLA, F. & ARMSTRONG, C. M. (1977). Inactivation of the sodium channel. I. Sodium current experiments. *J. gen. Physiol.* **70**, 549–566.

CLAY, J. R. & SHLESINGER, M. F. (1982). Delayed kinetics of squid axon potassium channels do not always superpose after time translation. *Biophys. J.* **37**, 677–680.

DiFRANCESCO, D. (1981*a*). A new interpretation of the pace-maker current in calf Purkinje fibres. *J. Physiol.* **314**, 359–376.

DiFrancesco, D. (1981*b*). A study of the ionic nature of the pace-maker current in calf Purkinje fibres. *J. Physiol.* **314**, 377–393.

DiFrancesco, D. (1982). Block and activation of the pace-maker channel in calf Purkinje fibres: effects of potassium, caesium and rubidium. *J. Physiol.* **329**, 485–507.

DiFrancesco, D. & Ferroni, A. (1983). Delayed activation of the cardiac pacemaker current and its dependence on conditioning pre-hyperpolarizations. *Pflügers Arch.* **396**, 265–267.

Dubois, J. M. (1981). Simultaneous changes in the equilibrium potential and potassium conductance in voltage clamped Ranvier node in the frog. *J. Physiol.* **318**, 279–295.

Frankenhaeuser, B. (1963). A quantitative description of potassium currents in myelinated nerve fibres of *Xenopus laevis*. *J. Physiol.* **169**, 424–430.

Goldman, L. & Schauf, C. L. (1973). Quantitative description of sodium and potassium currents and computed action potentials in *Myxicola* giant axons. *J. gen. Physiol.* **61**, 361–384.

Hagiwara, S. & Byerly, L. (1981). Calcium channel. *A. Rev. Neurosci.* **4**, 69–125.

Hart, G. (1983). The kinetics and temperature dependence of the pace-maker current i_f in sheep Purkinje fibres. *J. Physiol.* **337**, 401–416.

Hill, T. L. & Chen, Y. (1971). On the theory of ion transport across the nerve membrane. II. Potassium ion kinetics and cooperativity (with $x = 4$). *Proc. natn. Acad. Sci. U.S.A.* **68**, 1711–1715.

Hille, B. (1973). Potassium channel in myelinated nerve. *J. gen. Physiol.* **61**, 669–686.

Hodgkin, A. L. & Huxley, A. F. (1952). A quantitative description of membrane current and its application to conduction and excitation in nerve. *J. Physiol.* **117**, 500–544.

Isenberg, G. (1976). Cardiac Purkinje fibres: Cs as a tool to block inward rectifying potassium currents. *Pflügers Arch.* **365**, 99–106.

Julian, F. J., Moore, J. W. & Goldman, D. E. (1962). Current–voltage relations in the lobster giant axon membrane under voltage-clamp conditions. *J. gen. Physiol.* **45**, 1217–1238.

McAllister, R. E., Noble, D. & Tsien, R. W. (1975). Reconstruction of the electrical activity of cardiac Purkinje fibres. *J. Physiol.* **251**, 1–59.

Noble, D. & Tsien, R. W. (1968). The kinetics and rectifier properties of the slow potassium current in cardiac Purkinje fibres. *J. Physiol.* **195**, 185–214.

Palti, Y., Ganot, G. & Stämpfli, R. (1976). Effect of conditioning potential on potassium current kinetics in the frog node. *Biophys. J.* **16**, 261–273.

Trautwein, W. (1973). Membrane currents in cardiac muscle fibres. *Physiol. Rev.* **53**, 793–835.